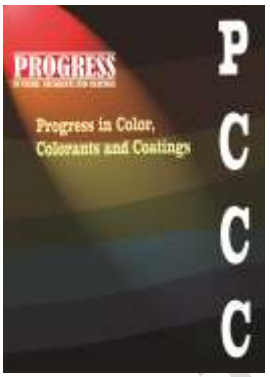
ACCEPTED MANUSCRIPT

Accepted Manuscript



Title: Development of Highly Efficient Separators for Li-Ion Batteries Composed of Chain-Extended Poly(Butylene Adipate-co-Terephthalate), High Density Polyethylene, and Polyethylene-Grafted-Maleic Anhydride Using Gravure Printing Method

Authors: Sajad Rasouli, Maryam Arshadi, Maryam Ataeefard

Manuscript number**: PCCC-2606-1512**

To appear in: Progresss in Color, Colorants and Coatings

Received: 6 June 2026

Final Revised: 6 October 2026

Accepted: 12 October 2026

Please cite this article as:

S. Rasouli, M. Arshadi, M. Ataeefard, Development of Highly Efficient Separators for Li-Ion Batteries Composed of Chain-Extended Poly(Butylene Adipate-co-Terephthalate), High Density Polyethylene, and Polyethylene-Grafted-Maleic Anhydride Using Gravure Printing Method, Prog. Color, Colorants, Coat., 20 (2027) XX-XXX.

DOI: 10.30509/pccc.2026.167810.1512

This is a PDF file of the unedited manuscript that has been accepted for publication. The manuscript will undergo copyediting, typesetting, and review of the resulting proof before it is published in its final form

ACCEPTED MANUSCRIPT

Development of Highly Efficient Separators for Li-Ion Batteries Composed of Chain-Extended Poly(Butylene Adipate-co-Terephthalate), High Density Polyethylene, and Polyethylene-Grafted-Maleic Anhydride Using Gravure Printing Method

S. Rasouli[1], M. Arshadi[2], M. Ataeefard[3*]

[1] Polymer Research Group, Department of Chemical, Polymeric and Petrochemical Technologies Development, Research Institute of Petroleum Industry (RIPI), P.O. Box 14856-13111, Tehran, Iran

[2] Department of Polymer Engineering Science and Research Branch, Islamic Azad University, P.O. Box: 14778-93855, Tehran, Iran

[3] Department of Printing Science and Technology, Institute for Color Science and Technology, P.O. Box: 32465-654, Tehran, Iran

ataeefard-m@icrc.ac.ir

Accepted Manuscript

Abstract

In this work, a mixture of biodegradable poly(butylene adipate-co-terephthalate) (PBAT) and high-density polyethylene (HDPE) was prepared to fabricate highly efficient nanoporous separators for lithium-ion batteries (LIBs) using a printing technique. To address the ecological concerns associated with non-biodegradable polyolefin separators, this work explores the incorporation of poly(butylene adipate-co-terephthalate) (PBAT) into polyethylene (PE) matrices as a potential pathway toward reducing petroleum-derived plastic content in lithium-ion battery components. A polyethylene-grafted-maleic anhydride (PE-g-MA) compatibilizer improved the miscibility between PBAT and

ACCEPTED MANUSCRIPT

HDPE, resulting in a porous structure with uniformly distributed spherical nano-cavities with a pore size of 108 nm, porosity of ~40%, and a hole number density of 17.54 μm^{-2} (or 17.54 holes/μm^2). The optimum HDPE content of 25 wt.% resulted in improved wettability, favorable microstructural characteristics, and high electrolyte absorption (~106%). Among the investigated blend compositions, the BE50 membrane (containing 25 wt.% HDPE) exhibited the most favorable trade-off between open pore structure, electrolyte wettability, and ionic transport kinetics, achieving an ionic conductivity of 2.26 $mS.cm^{-1}$ and low interfacial resistance. The achieved separator has higher ionic conductivity than several commercial PE separators reported in the literature under comparable testing conditions.

Keywords: Lithium-ion battery (LIB); chain extension reaction; poly(butylene adipate-*co*-terephthalate) (PBAT); polyethylene-*grafted*-maleic anhydride (PE-g-MA); gravure printing

1. Introduction

In recent decades, the consumption of fossil fuels has contributed to climate change, leading to significant climatic and environmental concerns [1]. To address this issue, these fuels should be replaced by renewable energy sources and energy storage devices [2]. Among the most widely used energy storage devices, lithium-ion batteries (LIBs) provide high cycle performance, high energy density, and reasonable cost [3, 4]. LIBs typically consist of four key components: (i) a cathode electrode, (ii) an anode electrode, (iii) an electrolyte, and (iv) a separator [5]. The electrodes determine the LIB's energy

ACCEPTED MANUSCRIPT

density, while the electrolyte enables ion transport between the electrodes.

The separator is used to facilitate ion transport and prevent physical contact between the cathode and anode. In other words, as a membrane, it facilitates the penetration of Li^+ ions within the electrolyte, and also inhibits direct electron transfer between the electrodes, thereby preventing short circuits [6]. Among porous and insulating materials widely used for the fabrication of effective battery separators, polymers have been identified as promising candidates [7]. For this purpose, polyethylene (PE) is highly suitable owing to its high mechanical strength, broad electrochemical stability, low manufacturing cost, and good processability [8].

Several investigations have been reported on the manufacturing and modification of PE-based LIB separators [9-12]. Jiang et al. [13] prepared a multilayer separator by coating thin layers of a PE/aluminum oxide (PE/Al_2O_3) composite on both sides of a PE separator using a casting technique. Their results showed that the PE/Al_2O_3 layers improved the separator wettability by 407.23% and reduced the thermal shrinkage to around 1%. Lee et al. [14] reported that the polydopamine coating on the PE surface improved the power capability of the separator by up to 40% and enhanced the cycle performance by 290% compared to pure PE. Kim et al. [15] employed a plasma treatment method to apply acrylonitrile (AN) on the surface of a PE-based separator. They demonstrated that an increase in surface polarity enhanced the separator wettability due to the plasma-induced acrylonitrile coating on the PE surface. Jo et al. [16] proposed the surface modification of PE via the introduction of imine functional groups—through a reaction between carbonyl and amine groups during separator production—to improve its wettability and thermal characteristics. Chen et al. [17] applied titanium oxide nanorods to modify the surface of

Accepted Manuscript

ACCEPTED MANUSCRIPT

a PE-based separator, achieving a 4.5% reduction in thermal shrinkage rate using a coating with ~ 0.6 mg/cm^2 of nanorods.

Despite these advancements in mechanical, thermal, and electrochemical properties, significant challenges persist regarding the environmental impact [18] and the non-biodegradable nature of PE-based separators [19]. Given that the demand for LIBs is forecasted to reach 4700 GWh by 2030 [20], the resulting surge in PE consumption poses a critical environmental threat, particularly post-service life. Consequently, there is an urgent necessity to transition toward biodegradable alternatives. Among potential candidates, poly(butylene adipate-co-terephthalate) (PBAT) has garnered substantial interest in both medical and industrial sectors, even surpassing polylactic acid (PLA) in certain applications [21]. PBAT exhibits rapid biodegradation, capable of complete degradation in less than two months with a notable rate of 2.16 day^{-1} [22]. While incorporating PBAT into LIB separators can substantially mitigate environmental impacts, this approach remains insufficiently explored. Moreover, it is recognized that the presence of HDPE in such blends may limit complete biodegradability; thus, the developed system is intended as a partially biodegradable alternative designed to minimize the ecological footprint compared to conventional petroleum-based separators.

This study investigates the influence of the PBAT/PE blending ratio on the surface properties, microstructure, wettability, ionic diffusivity, and electrical response of fabricated PBAT-based LIB separators. Maleic anhydride (MA) and dicumyl peroxide (DCP) were incorporated into the PBAT/PE blend system with the intention of inducing reactive compatibilization and potential chain-extension pathways. While such reactive formulations are widely reported to promote macromolecular coupling and interfacial

ACCEPTED MANUSCRIPT

adhesion, the exact extent of chain extension in the present blend was not directly quantified and represents a proposed mechanism based on established literature. Unlike conventional methods, this research employs a gravure printing technique to fabricate thin-film separators with highly controlled microstructures. Compared to electrospinning, which is often limited by low throughput, high energy consumption, and scalability issues, gravure printing enables efficient, continuous roll-to-roll manufacturing. Furthermore, in comparison to solvent casting, gravure printing offers superior control over coating thickness, reduced solvent consumption, shorter processing times, and enhanced coating uniformity. These advantages, combined with its compatibility with large-scale industrial production and minimal material waste, make gravure printing a highly attractive and economically viable approach for the mass production of sustainable LIB separators [23- 25].

2. Experimental

2.1. Raw materials

Poly(butylene adipate-*co*-terephthalate) (PBAT, Ecoflex F blend C1200) with density of 1.26 g/cm^3, melting point of 115°C, and melt flow rate (MFR) of 320 mg/min (2.16 kg at 190°C)was purchased from BASF Chemical Co. (Ansan, Korea). High-density polyethylene (HDPE, 7000F) with MFR of 4 mg/min (2.16 kg at 160°C), density of 0.952 g/cm^3, and melting point of 130°C was supplied from Mehr Petrochemical Co. (Tehran, Iran). PE-*grafted*-maleic anhydride (PE-*g*-MA) containing 1.0 % maleic anhydride with density of 0.94 g/cm^3 and drop point of 115°C was provided from Karangin Co. (Iran). Dioctyl phthalate (DOP, ≥99.5%), methanol (≥ 99.9%), ethanol

ACCEPTED MANUSCRIPT

(>99.0%), ethyl methyl carbonate (EMC, 99.0%), lithium hexafluorophosphate ($LiPF_6$, 98.0%), dicumyl peroxide (DCP, 99.0%), ethylene carbonate (EC, 98.0%), and maleic anhydride (MA, 99.0%) were obtained from Merck (Germany).

2.2. PBAT modification via chain extension reaction

The MA powder and PBAT granules were dried in an air-circulating oven at 60 °C for 8 h. Subsequently, a mixture containing PBAT, 0.5 phr DCP as an initiator (parts per hundred parts of PBAT), and 1 phr MA as a chain extender (CE) was melt-compounded using an internal mixer (BP-8172-B 1L, Dongguan Baopin Precision Instruments Co., China) at 160 °C and a rotor speed of 50 rpm for 6 min.

2.3. Fabrication of the separator

Thin PBAT/PE-based films were prepared by employing a gravure printing method. As illustrated in Fig. 1, the separator was manufactured through five consecutive steps: (i) melt-blending different ratios of the CE-modified PBAT with a 1:1 weight ratio of HDPE to PE-g-MA (Table 1) and 30 wt.% DOP oil using a single-screw extruder (L/D = 26, KEX model, Karaj, Iran) operating at 30 rpm (the barrel temperatures from the feeding zone to the die were set at 100 °C, 160 °C, and 155 °C, respectively); (ii) transferring the molten blend into a container heated to 155 °C at a controlled mass flow rate utilizing a doctor blade-equipped rotogravure cylinder; (iii) calender-compacting the blend using impression cylinders to obtain a uniform film with a thickness of ~100 μm; (iv) stretching the film to reduce its thickness to 20–30 μm via stretcher cylinders at 55 °C; and (v) extracting the DOP oil from the film by immersing the prepared samples in ethanol for 2

ACCEPTED MANUSCRIPT

days.

In the present study, the gravure printing process was performed at a printing speed of 0.6 $m.min^{-1}$. A doctor blade angle of 60° was employed under a low-to-moderate contact pressure. These processing conditions were maintained constant for all samples throughout the study to ensure reproducibility and enable a reliable comparison of the resulting separator properties.

Table 1. Detailed formulation of CE-PBAT/HDPE/PE-*g*-MA separators for LIB

Sample	**PBAT (*wt.*%)**	**MA* (*phr*)**	**DCP* (*phr*)**	**HDPE (*wt.*%)**	**PE-*g*-MA (*wt.*%)**	**DOP oil** (*wt.*%)**
BE100	100	1	0.5	0.0	0..0	30
BE75	75	1	0.5	12.5	12.5	30
BE50	50	1	0.5	25.0	25.0	30
BE25	25	1	0.5	37.5	37.5	30
BE0	0	1	0.5	50.0	50.0	30

* Parts per hundred PBAT
** [DOP/(PBAT+HDPE+PE-g-MA)]

The separators were designated as BEz, where z represents the weight percentage (wt.%) of CE-modified PBAT.

Accepted Manuscript

2.4. Extraction evaluation

The DOP extraction efficiency (EA) from the CE-PBAT/HDPE/PE-g-MA blends was determined gravimetrically using seven replicates for each formulation. The samples were weighed before immersion (w_i), immersed in ethanol for 2 days to extract the plasticizer, dried to constant weight, and reweighed (w_e) according to Eq. 1 [4]:

$$EA = \frac{w_i - w_e}{0.3\, w_i} \times 100 \qquad (1)$$

ACCEPTED MANUSCRIPT

The term $0.3w_i$ represents the total initial mass of DOP incorporated into the blend, corresponding to a DOP-to-polymer weight ratio of 30:70 (30 wt.% DOP) during the melt-compounding stage.

2.5. Separator film characterization

Fourier-transform infrared (FTIR) spectra were recorded on a Shimadzu spectrophotometer (Model 8300 E, Japan) using KBr pellets over the wavenumber range of 400-4000 cm^{-1}. The morphology of the prepared separators was characterized via field-emission scanning electron microscopy (FESEM, FEI Co., USA) operated at an accelerating voltage of 10 kV after gold sputter-coating the sample surfaces. The porosity (P_k) of the separators was evaluated through the methanol uptake method using seven specimens for each formulation. The dry films (w_e) were immersed in methanol for 2 days at ambient temperature, and their wet weights (w_f) were measured immediately after removing surface liquid [26] (Eq. 2):

$$P_k = \frac{w_f - w_e}{\rho_s V_p} \times 100 \qquad (2)$$

where ρ_s is the density of the solvent (methanol) and V_p denotes the geometric volume of the dry separator. Using this equation, the interconnected porosity of the separator, which facilitates ion transport, can be accurately determined.

The contact angle and the surface wettability of the prepared films were evaluated using a DSA100 optical instrument (Hamburg, Germany) and deionized water droplets based on DIN EN ISO 19403-2, averaged across seven samples for each formulation. Although the water contact angle provides a general indication of surface wettability, it does not fully reflect the wetting behavior with battery electrolytes. Therefore, electrolyte uptake tests

ACCEPTED MANUSCRIPT

using a carbonate-based electrolyte were also performed to provide a more application-relevant evaluation.

An electrolyte solution of 1 M $LiPF_6$ in a 1:1 mixture of EC/EMC was prepared in a glovebox under an Ar atmosphere. The electrolyte absorption percentage (A) was calculated based on the initial film weight (w_e) and its weight after immersion in the electrolyte for 24 h (w_{ee}), using an average of seven samples for each formulation (Eq. 3):

$$A = \frac{w_{ee} - w_e}{w_e} \times 100 \quad (3)$$

2.6. LIB electrochemical performance

The electrochemical performance of the prepared separators was evaluated using CR2032-type coin cells assembled inside an argon-filled glovebox. The cells were fabricated by sandwiching the electrolyte-soaked CE-PBAT/HDPE/PE-g-MA separator between a graphite anode and a lithium nickel cobalt manganese oxide ($LiNi_{1/3}Co_{1/3}Mn_{1/3}O_2$, NCM111) cathode. The electrode configuration and electrolyte composition were maintained constant for all assemblies to ensure consistency. Electrochemical impedance spectroscopy (EIS) was performed using an electrochemical workstation by applying a 10 mV AC perturbation over a frequency range of 0.1 Hz to 100 kHz. The resulting Nyquist plots were analyzed using a simplified equivalent circuit model comprising electrolyte bulk resistance, charge-transfer resistance, and interfacial constant-phase elements, assuming an ideal electrode–electrolyte interface and a homogeneous separator microstructure [27]. Further details regarding the electrochemical measurement protocol are provided in [28].

The ionic conductivity (σ) of the electrolyte-soaked separators was calculated according

ACCEPTED MANUSCRIPT

to Eq. 4 [28]:

$$\sigma = \frac{L}{Rb \times A} \quad (4)$$

where L is the separator thickness, A is the effective electrode area, and Rb is the bulk resistance obtained from the high-frequency intercept of the Nyquist plot. All measurements were carried out using an identical electrolyte composition, uniform separator dimensions, and consistent cell assembly conditions to ensure reliable comparison among the samples.

3. Results and Discussion

To mitigate the environmental burden associated with non-biodegradable polyolefin separators in spent LIBs, various blend ratios of biodegradable PBAT and HDPE were investigated to optimize separator performance. While HDPE is widely utilized in commercial separators [29], its nonpolar nature leads to thermodynamic immiscibility and poor interfacial adhesion when blended with polar PBAT [30]. To overcome this phase incompatibility, maleic anhydride-grafted polyethylene (PE-g-MA) was incorporated as a reactive compatibilizer (Table 1). The nonpolar polyethylene backbone of PE-g-MA co-crystallizes and entangles with the neat HDPE matrix, whereas its reactive anhydride groups interact chemically with the hydroxyl and carboxyl terminal groups of PBAT. Furthermore, to enhance PBAT molecular weight and melt strength, reactive chain extension was facilitated using MA and dicumyl peroxide (DCP) as a free-radical initiator prior to melt-blending with the HDPE/PE-g-MA phase.

During chain extension, PBAT chains are joined through the reaction of their terminal hydroxyl (–OH) groups with the opened anhydride ring of MA [31], markedly improving

ACCEPTED MANUSCRIPT

the thermal and mechanical properties of the polymer [32]. Additionally, radicals generated by the DCP initiator provide reactive sites on the PBAT backbone, converting the C=C double bonds of MA into C–C single bonds and effectively grafting MA onto PBAT. The optimal loadings of MA and DCP to produce CE-PBAT without compromising processability were chosen according to Nam et al. [33]. In their study using FTIR analysis, varying the MA content from 0.5 to 3 phr revealed that 1 phr MA achieved the best combination of tensile strength and elongation at break. Furthermore, 1 phr MA reduced the glass transition temperature (T_g) to 84.3 °C, facilitating melt processing, whereas increasing the MA content to 1.5 phr elevated the T_g to 87.1 °C (a 3.3% increase). These observations align with findings by Arruda et al. [34], who also demonstrated the beneficial effects of DCP and MA on the thermal and mechanical performance of PBAT-based formulations.

3.1. Extraction of DOP oil

The addition of DOP oil during extrusion and its subsequent solvent extraction via ethanol induce the formation of a porous structure in the CE-PBAT/PE-g-MA/HDPE separators. The mass of each sample prior to (w_i) and following (w_e) DOP extraction, along with the calculated extraction percentage (EA) for all PBAT/PE-based films, is presented in Table 2.

Accepted Manuscript

ACCEPTED MANUSCRIPT

Table 2. The weight of BE*z* film samples before (w_i) and after (w_e) DOP extraction in ethanol and their calculated extraction percentage (*EA*).

Sample	w_i (mg)	w_e (mg)	*EA* (%)
BE100	70.4±0.2	49.5±0.1	99.25
BE75	95.3±0.3	67.0±0.2	99.21
BE50	88.2±0.3	62.0±0.2	99.26
BE25	89.7±0.3	63.0±0.2	99.27
BE0	121.0±0.3	85.0±0.3	99.26

As shown in Table 2, the extraction results indicate that more than 99% of DOP was successfully removed from all samples. This confirms that the residual plasticizer content is negligible, preventing any detrimental effects on the membrane morphology as well as the environmental and electrochemical performance of the separators. The reliability of the DOP extraction process was further investigated by FTIR analysis, as shown in Figure 1. The BE0 sample was selected as a representative specimen because the EA values for all membranes were nearly identical (~99.25%).

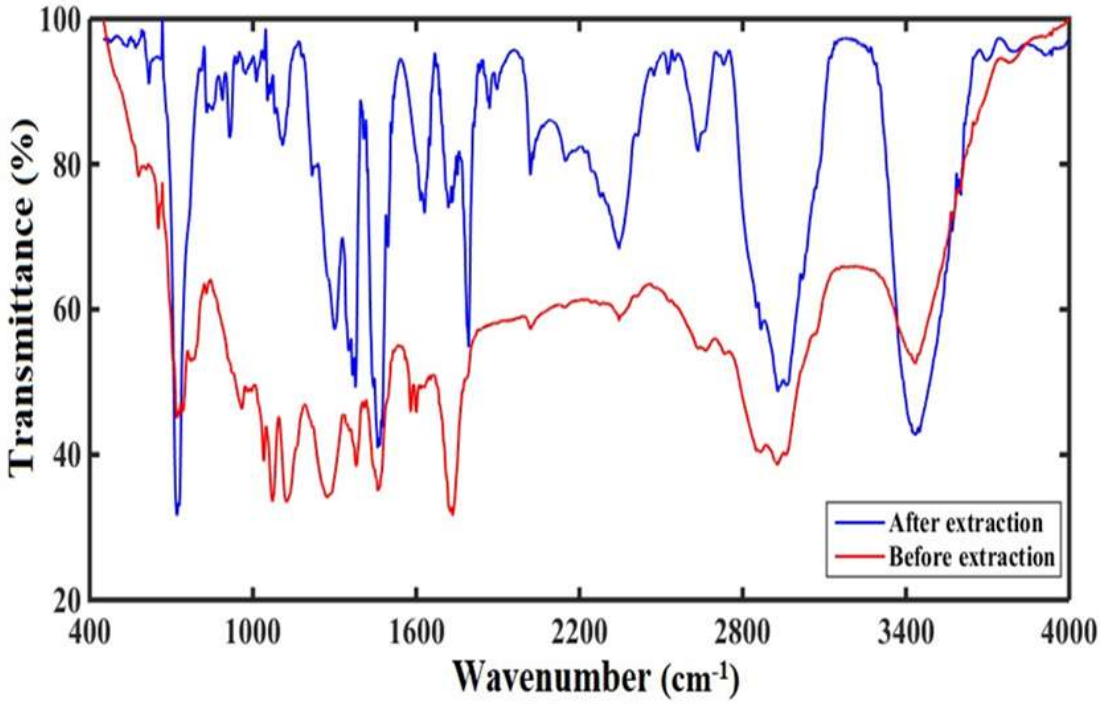


Figure 1. FT-IR spectra showing DOP removal from BE0 separator.

ACCEPTED MANUSCRIPT

The sharp peak at 1734 cm^{-1} is attributed to the stretching of carbonyl (C=O) groups in both PE-g-MA and DOP. The peaks at 2869, 2930, and 2962 cm^{-1} correspond to the stretching vibrations of $C(sp^3)$–H bonds in both components. Additional characteristic peaks appear at 3438 cm^{-1} (O–H stretching), 1280–1300 cm^{-1} (C–O stretching), 714 cm^{-1} (methylene rocking), and 1452 cm^{-1} (methylene scissoring vibrations). Since these peaks are present both before and after DOP removal, they cannot serve to evaluate the extraction efficiency. Instead, the fingerprint region was used to identify residual plasticizer [35]. Tham et al. [35] demonstrated that DOP possesses unique spectral bands in the fingerprint region at 581, 655, 703, and 1074 cm^{-1}, along with doublet peaks at 1580 and 1603 cm^{-1}. According to Fig. 1, these characteristic peaks disappear entirely after extraction, demonstrating that the DOP was successfully removed.

3.2. Microstructure evaluation

FESEM images of the CE-PBAT/HDPE/PE-g-MA samples following DOP extraction, with CE-PBAT contents varying from 100 wt.% to 0 wt.%, are shown in Figure 2a–e. As depicted in Figure 2a, the BE100 sample exhibits a spherical pore morphology after DOP extraction. Table 3 lists the average pore diameter (d_{avg}), standard deviation (SD) of pore size, pore number density (ND), and porosity percentage (P_k) obtained from the FESEM micrographs. It is evident that the optimal pore characteristics are obtained for the BE100 with an d_{avg} of 68.51 nm, SD of 45.64 nm, and ND of 16.70 μm^{-2}.

Accepted Manuscript

ACCEPTED MANUSCRIPT

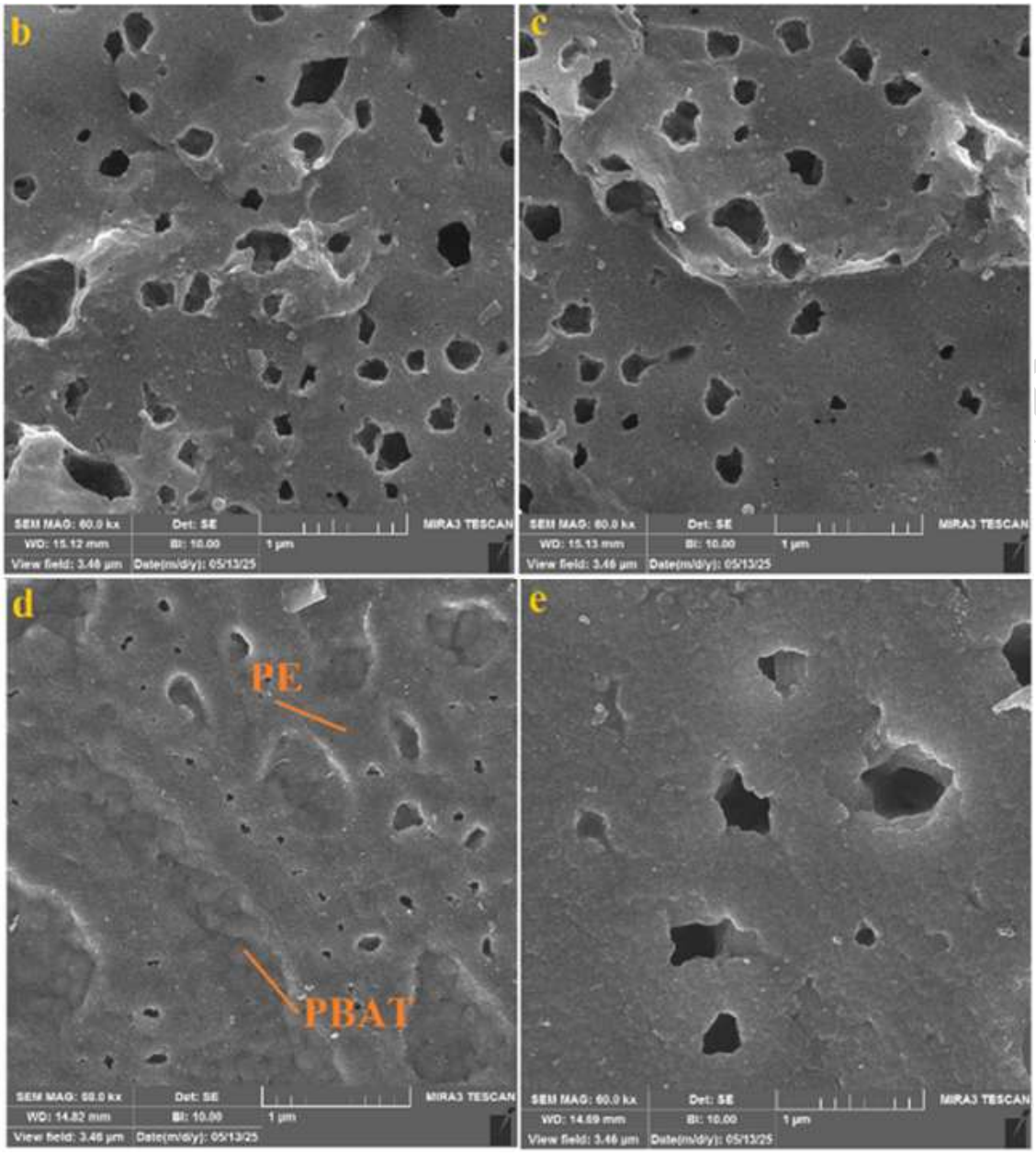


Figure 2. FESEM images showing surface morphology of different CE-PBAT/HDPE/PE-g-MA separators: (a) BE100 presented in Fig. S1 (Supporting Information) [36], (b) BE75, (c) BE50, (d) BE25, and (e) BE0.

ACCEPTED MANUSCRIPT

Table 3. The average pore size (d_{avg}), its standard deviation (SD), the number density (ND) of cavities, and the porosity percentage (P_k) derived from FESEM images

Sample	d_{avg} (nm)	SD of pore size (nm)	ND of cavities (μm^{-2})	P_k (%)
BE100	68.51	45.64	16.70	42.9±0.4
BE75	136.24	109.54	8.43	40.2±0.4
BE50	108.97	96.76	17.54	38.1±0.4
BE25	123.27	119.80	3.92	18.4±0.2
BE0	227.24	154.65	1.50	25.7±0.2

Figure 3 shows the probability density function (PDF) curves of pore diameter for the fabricated CE-PBAT/HDPE/PE-g-MA separators. Among all specimens, BE100 (Figure 3a) exhibits the sharpest peak and narrowest size distribution, confirming superior pore dimension uniformity.

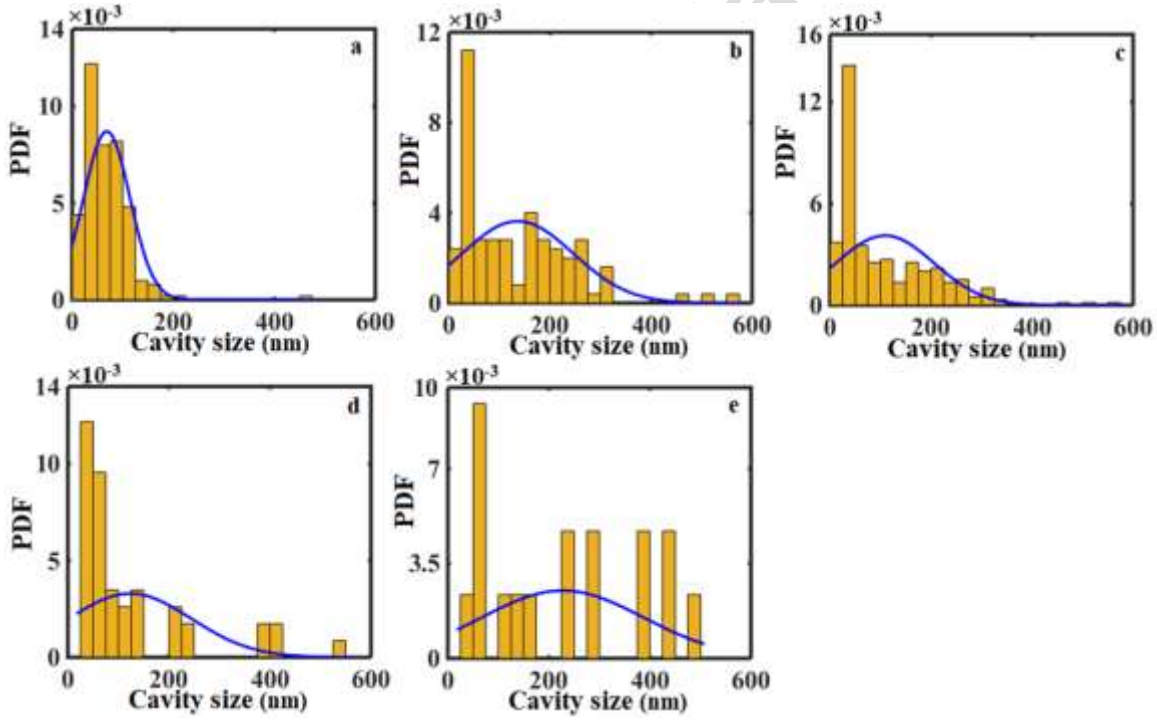


Figure 3. PDF profiles of pore size for different CE-PBAT/HDPE/PE-g-MA separators: (a) BE100, (b) BE75, (c) BE50, (d) BE25, and (e) BE0.

A lower standard deviation is indicative of a more uniform pore size distribution. The d_{avg} of the samples is below 100 nm, considerably smaller than that reported for polyolefin-

ACCEPTED MANUSCRIPT

based structures in previous studies [3-5], which can significantly enhance the performance of LIBs. Previous studies utilizing similar materials and manufacturing methods [3-5] have reported oval-shaped cavities with sizes typically in the micrometer range. According to Table 3, decreasing the amount of CE-PBAT to 75 wt.% (BE75) and 50 wt.% (BE50) resulted in average pore sizes of 136.24 ± 109.54 nm and 108.97 ± 96.76 nm with number densities of 8.43 μm^{-2} and 17.54 μm^{-2}, respectively. This change can be resulted from a decrease in the homogeneity of the polymeric matrix. In addition, DOP molecules distribute non-uniformly due to the differences in the properties of the blended polymers. The chemical nature of the DOP (with aromatic ring and ester groups [37]) is almost closer to the CE-PBAT part consisting of aromatic ring and esters [38] than PE, leading to more embedding of DOPs in CE-PBAT compared to PE. This phenomenon increased the SD of the pore size. This occurs because PBAT exhibits higher affinity for the absorption of DOP than PE. As shown in Fig. 3, the lower CE-PBAT content leads to an increase in the width of the PDF profiles. However, the pore size and its distribution remain acceptable down to 50 wt.% CE-PBAT. Further reducing the CE-PBAT percentage makes the morphology of the cavities more heterogeneous (Figure 2d and 2e). Unlike BE100, BE75, and BE50 samples, the BE25 sample exhibits phase separation with numerous blocked cavities (Figure 2d,), which leads to lower ion transfer efficiency in LIBs. In addition, at low CE-PBAT content, the PE-*g*-MA is not capable of avoiding this phase separation. Finally, the HDPE/PE-*g*-MA sample without CE-PBAT (BE0) exhibits a porous structure with d_{avg} of 227.24±154.65 nm and ND of 1.50 μm^{-2}, which are not satisfactory for LIB applications.

Table 3 also presents the porosity (P_k) values of the different CE-PBAT/HDPE/PE-g-MA

ACCEPTED MANUSCRIPT

separators calculated via Eq. 2. The favorable compatibility between DOP and PBAT resulted in the highest P_k value for the BE100 sample following DOP extraction, providing an appropriate porous microstructure with uniform pore distribution for separator applications. Notably, the P_k value dropped by ~57% as the PBAT content decreased (from 42.9 ± 0.4% for BE100 to 18.4 ± 0.2% for BE25). Although BE0 showed higher porosity than BE25, it is inadequate for efficient lithium-ion transport owing to its low electrolyte uptake capability.

3.3. Contact angle measurement

Surface wettability of the separator determines how effectively the porous membrane absorbs liquid electrolyte, thereby significantly impacting its ionic conductivity in LIBs [39]. Herein, the wettability of the CE-PBAT/HDPE/PE-g-MA separators was assessed through dynamic contact angle (CA) measurements. Table 4 shows the contact angle results as a function of time for BE100, BE75, BE50, BE25, and BE0 samples, whereas Fig. 4 presents the determined CA values plotted as a function of wetting time (1, 5, and 10 s) for the BE100, BE75, BE50, BE25, and BE0 membranes.

Accepted Manuscript

Table 4. Contact angle results as a function of time for BE100, BE75, BE50, BE25, and BE0 samples.

Sample	**Contact angle (degree)**		
	1 (s)	5 (s)	10 (s)
BE100	80.9±0.5	80.5±0.8	79.9±0.0
BE75	81.8±0.0	80.5±0.0	80.1±0.0
BE50	81.9±0.2	79.7±1.1	78.7±0.3
BE25	92.5±0.0	91.8±0.0	89.6±0.0
BE0	93.4±0.5	92.7±0..3	91.0±0.5

ACCEPTED MANUSCRIPT

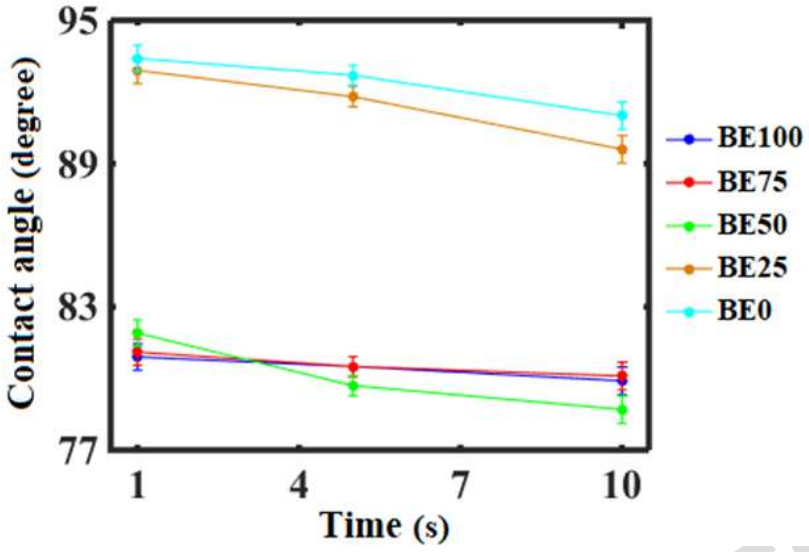


Figure 4. Plots of CA versus time for BE100, BE75, BE50, BE25, and BE0 samples.

As shown in Figure 4, BE100 and BE75 exhibit nearly the same initial CA value of ~80°, which falls within the hydrophilic range (<90°) owing to the high PBAT content governing the blend hydrophilicity. Therefore, these membranes are expected to demonstrate enhanced wettability toward polar liquid electrolytes [40]. However, the measured CA decreased progressively as the exposure time was extended to 10 s. In the BE50 sample, the initial CA increased by 1.2% relative to BE100 and BE75, mainly due to the higher content of nonpolar PE reducing matrix polarity. Interestingly, as time elapsed, the CA of BE50 decreased by 4% (from 81.9° to 78.7°), achieving an even lower angle than those of the BE100 and BE75 membranes. This phenomenon can be attributed to the porous architecture of the samples; as listed in Table 3, the ND of the pores in BE50 is markedly higher than in BE100 and BE75. Consequently, water molecules rapidly penetrate into the open pores, lowering the CA value, as reported by Paxton and Woodruff [41]. With a further decline in PBAT content, the CA increases into the hydrophobic range, which is undesirable for separator wetting. Consequently, the lowest

ACCEPTED MANUSCRIPT

CA value (78.7°) and highest surface wettability were obtained for the BE50 sample after 10 s. The wettability characteristics evaluated through the A parameter (Eq. (3)) are presented in Table 5.

Table 5. The results of electrolyte absorption test

Sample	w_e (mg)	w_{ee} (mg)	A (%)
BE100	49.5±0.1	113.2±0.3	128.7
BE75	67.0±0.2	138.2±0.3	106.4
BE50	62.0±0.2	123.1±0.3	98.7
BE25	63.0±0.2	84.9±0.3	34.8
BE0	85.0±0.3	135.2±0.3	59.1

According to Table 5, the BE100 sample exhibited the highest A value of 128.7%, stemming from its high bulk porosity and favorable microstructural characteristics, as detailed in Table 3. Nevertheless, the A value declined as the PBAT content in the formulation was reduced. As discussed earlier, this behavior originates from the alteration of pore morphology in the presence of higher PE fractions. Among all specimens, BE75 and BE50 achieved an optimal balance for LIB separator applications, offering both efficient electrolyte wettability and improved mechanical properties provided by the PE component [34].

The electrolyte uptake results confirm the favorable affinity of the developed separators toward carbonate-based liquid electrolytes. However, complementary metrics—including electrolyte absorption kinetics and electrolyte retention capability under mechanical compression—were not evaluated in the present study and should be addressed in future investigations for a more comprehensive assessment under realistic battery operating conditions.

Accepted Manuscript

ACCEPTED MANUSCRIPT

3.4. Electrical performance

Based on the morphology and wettability results obtained across the CE-PBAT/HDPE/PE-g-MA formulations, BE50 was selected as the optimal separator for lithium-ion battery fabrication. Because within the scope of the microstructural and initial electrochemical parameters evaluated in this work, BE50 demonstrated the most balanced performance in terms of pore density, wetting kinetics, and ionic conductivity. In the next step, EIS and linear sweep voltammetry (LSV) techniques were employed to examine the electrochemical performance of the assembled BE50-based cell. Figure 5 illustrates the Nyquist plot obtained from the EIS analysis for the BE50 separator over a range of frequencies, where Z' and Z'' denote the real and imaginary parts of impedance, respectively.

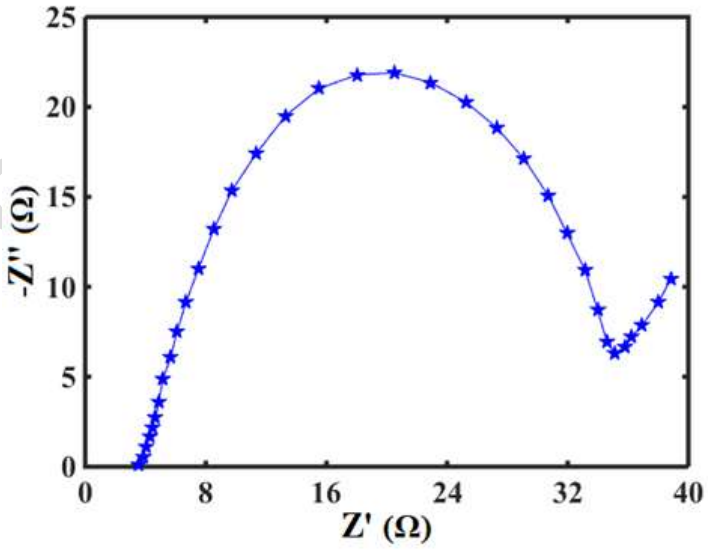


Figure 5. Nyquist plot obtained for the BE50-based LIB.

According to Figure 5 and the methodology described by Islam et al. [42], the total ohmic resistance of the electrolyte and separator was 3.55 Ω, whereas the interfacial charge-

ACCEPTED MANUSCRIPT

transfer resistance for Li^+ transport was 31.54 Ω. The electrochemical impedance data were interpreted in terms of bulk electrolyte resistance and interfacial charge-transfer resistance, avoiding direct assumptions regarding physical layer thicknesses. The resulting ionic conductivity for the BE50-based separator was calculated to be 2.26 $mS.cm^{-1}$, indicating excellent ion conduction capability.

In addition, the voltammetric behavior of the BE50-based LIB was evaluated using voltammetric analysis, with the corresponding current–potential profile shown in Figure 6. The initial descending trend in the cathodic region indicates electrochemical reduction (lithiation). In contrast, the anodic peaks at higher potentials reflect oxidation processes associated with Li^+ extraction from the electrode lattice. The I–V curve not only demonstrates the reversibility of the lithiation–delithiation processes, but also reveals that the porous structure of the BE50 separator facilitates rapid ion transport during redox cycling, confirming robust electrochemical stability. Furthermore, as the potential increases, the current approaches near-zero values, indicating the absence of detrimental electrolyte decomposition. The specific capacities obtained during delithiation and lithiation were 87.19 $mAh.g^{-1}$ and 81.73 $mAh.g^{-1}$, respectively. It is worth noting that voltammetric measurements primarily provide qualitative kinetic information rather than precise quantitative capacity determinations.

Accepted Manuscript

ACCEPTED MANUSCRIPT

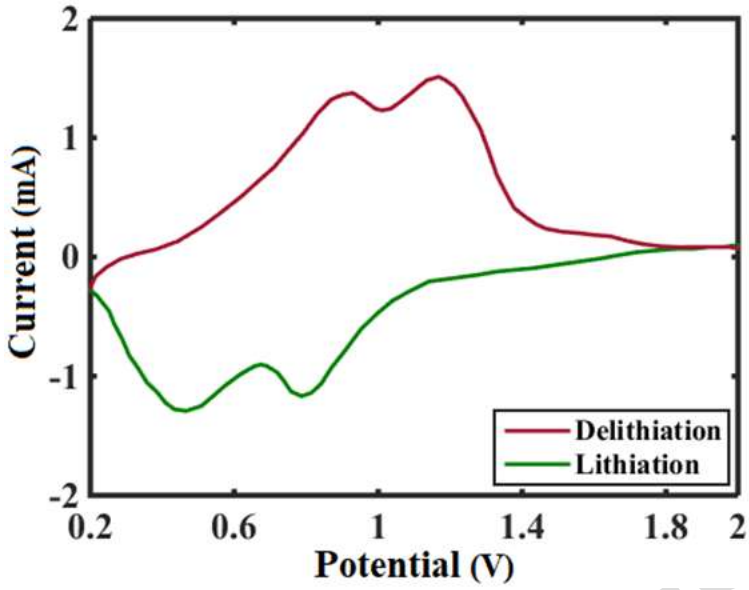


Figure 6. I-V plot obtained from LSV technique demonstrating the electrochemical response of the BE50-based LIB

The LSV analysis provides critical information regarding the electrochemical stability of the separator–electrolyte system. The absence of any sudden surge in current density within the investigated voltage range indicates that undesirable electrolyte decomposition and parasitic electrochemical reactions were effectively suppressed. Therefore, the developed BE50 separator exhibits robust electrochemical stability under the tested operational conditions. Notably, while LSV measurements reliably confirm anodic stability, direct quantification of ionic transport efficiency and battery capacity relies on integrated EIS and galvanostatic cycling evaluations.

As a key parameter of a LIB [43], which governs ion diffusion across the separator, the ion conductivity of the BE50-based LIB separator fabricated in this work is compared with the data reported by other researchers (Figure 7).

ACCEPTED MANUSCRIPT

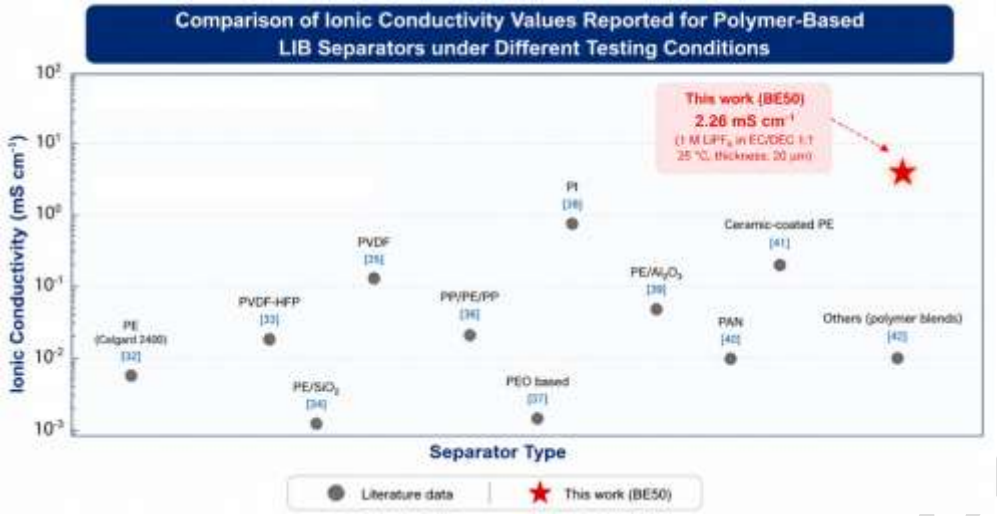


Figure 7. Ion conductivity comparison between the BE50-based LIB (this study) and polymer-based separators reported in the literature [44-56].

According to the comparison presented in the figure, the ionic conductivity obtained in the current work demonstrates competitive performance relative to previously reported polymer separators. The BE50-based separator achieved an ionic conductivity of 2.26 mS..cm^{-1}, which is notably higher than those reported for conventional PE-based (1.24 mS.cm^{-1} [4]) and PP-based (0.34 mS.cm^{-1} [3]) separators. Although direct benchmarking requires caution due to potential variations in electrolyte chemistry and cell configurations, these results highlight the enhanced ion-transport characteristics of the porous network. Ultimately, the selection of the BE50 formulation as the optimal separator relies on a comprehensive multi-criteria evaluation. While the BE75 membrane showed higher electrolyte uptake, BE50 delivered the most balanced combination of microstructural morphology, wettability, and robust electrochemical behavior.

Comparison with previously reported PBAT-based and bio-based separators indicates that the present membrane achieves comparable or enhanced ionic conductivity within similar porosity and thickness ranges. Although direct mechanical and thermal

ACCEPTED MANUSCRIPT

characterizations were not conducted in this study, existing literature establishes that chain extension and compatibilization significantly enhance thermomechanical stability, aligning well with the synthetic strategy employed here. From a sustainability perspective, integrating PBAT decreases dependence on fully petroleum-based feedstocks. While full biodegradability is precluded by the presence of the HDPE component, this hybrid strategy offers a meaningful environmental improvement. In addition, using ethanol as a green extraction solvent offers a low-toxicity processing pathway, where closed-loop solvent recovery can further reduce the overall environmental burden. Systematic end-of-life and degradation assessments remain vital subjects for subsequent investigations.

It should be noted that the observed improvements in melt integrity and phase morphology are plausibly associated with the reactive role of MA and DCP; however, these interfacial phenomena are discussed here as putative reaction pathways rather than directly verified molecular structures. While reactive processing with MA and DCP yielded favorable membrane morphology, direct verification of the chain-extension kinetics—via advanced rheological measurements, gel permeation chromatography (GPC), and targeted spectroscopic techniques—will be the subject of dedicated future investigations to decouple the specific contributions of grafting versus macromolecular extension.

4. Conclusions

In this research work, the developed separator provides a partially biodegradable alternative with reduced environmental impact compared to conventional polyethylene-

ACCEPTED MANUSCRIPT

based separators. The interactions of the CE-PBAT with the functional groups of MA and the dispersive non-bonded intermolecular interactions of the PE part of the compatibilizer with HDPE led to improved miscibility between PE and CE-PBAT. According to the FESEM images, a decrease in the CE-PBAT content from 100 *wt*.% to 75 *wt*.% created a nanoporous separator with the cavity size of 136.24 nm, porosity of 40.2% and a number density of the holes 8.43 $1/\mu m^2$. However, the cavity size is 99% higher than the pure CE-PBAT, and the porosity and the number density are 49% and 6% lower than the separator without PE, respectively. More reduction of PBAT, to 25 *wt*.%, formed a phase separation between the CE-PBAT and PE, leading to the lowest porosity of 18.4±0.2%. The wettability achievements indicated that a decrease in the PBAT component reduced the electrolyte absorption amount from 128.7% to 34.8% (a 73% reduction). Among the studied formulations, BE50 provided the most balanced performance and was therefore identified as the optimal separator. While wettability was primarily assessed using water CA and electrolyte uptake, further studies involving electrolyte CA and mechanical retention behavior are required for complete evaluation under practical operating conditions. Employing the BE50 separator resulted in an ion conductivity of 2.26 mS/cm for the LIB. Therefore, the developed separator represents a promising alternative to conventional PE separators, although direct benchmarking requires testing under identical experimental conditions for producing improved LIBs. It should be emphasized that biodegradation behavior was not experimentally investigated in the present study. Therefore, environmental benefits are discussed based on the intrinsic characteristics of the constituent materials rather than direct biodegradation measurements. While BE50 showed the highest ionic conductivity and lowest charge-transfer resistance among the

Accepted Manuscript

ACCEPTED MANUSCRIPT

prepared formulations, comprehensive mechanical assessments (puncture and tensile strength), thermal stability evaluations, and extended cycling tests are currently underway to fully validate its operational reliability in practical battery cells.

In this study, the influence of the proposed chemical and physical modification strategies on the microstructure and surface wettability of the developed polymer blend was investigated as a foundational step. This study demonstrates the technical feasibility of employing gravure printing technology for the fabrication of thin nanoporous separator membranes. Although the partial replacement of PE with PBAT offers a rationale for developing more sustainable membrane formulations, systematic biodegradation trials (e.g., standard soil-burial degradation) and life-cycle environmental assessments are required in future work to experimentally validate the ecological viability of these hybrid separators. Future investigations will focus on assessing key performance metrics, including mechanical tensile and puncture resistance, thermal dimensional stability, long-term battery cycling stability, biodegradation behavior, and the industrial scalability of the gravure-printing process.

ACCEPTED MANUSCRIPT

Supporting Information

The auxiliary information to support the claim presented in the main text was added to the supporting information (SI) (Fig. S1).

References

[1] Wuebbles DJ, Jain AK. Concerns about climate change and the role of fossil fuel use. FPT. 2001; 71:99-119. https://doi.org/10.1016/S0378-3820(01)00139-4

ACCEPTED MANUSCRIPT

[2] Khan MK, Raza M, Shahbaz M, Farooq U, Akram MU. Recent advancement in energy storage technologies and their applications. J Energy Storage. 2024; 92:112112. https://doi.org/10.1016/j.est.2024.112112

[3] Azizi Z, Fasihi M, Rasouli S. Enhancing polypropylene-based separator efficiency in lithium-ion batteries through maleic anhydride addition and corona radiation modification. Electrochim Acta. 2024; 507:145184. https://doi.org/10.1016/j.electacta.2024.145184

[4] Darvishi A, Fasihi M, Rasouli S. Modification of high-density polyethylene-based separator to improve lithium-ion battery performance using nano-silica and maleic anhydride. J Energy Storage. 2024; 100:113495. https://doi.org/10.1016/j.est.2024.113495

[5] Darvishi A, Rasouli S, Fasihi M. Optimizing HDPE separator properties through thermoplastic elastomer loading and manufacturing process for improved lithium-ion battery electrochemical performance. J Appl Electrochem. 2025; 55:583-593. https://doi.org/10.1007/s10800-024-02197-7

[6] Barbosa JC, Reizabal A, Correia DM, Fidalgo-Marijuan A, Gonçalves R, Silva MM, et al. Lithium-ion battery separator membranes based on poly(L-lactic acid) biopolymer. Mater. Today Energy. 2020; 18:100494. https://doi.org/10.1016/j.mtener.2020.100494

[7] Zhang H, Zhou MY, Lin CE, Zhu BK. Progress in polymeric separators for lithium ion batteries. RSC Adv. 2015; 5:89848-89860. https://doi.org/10.1039/C5RA14087K

[8] Gu QQ, Xue HJ, Li ZW, Song JC, Sun ZY. High-performance polyethylene separators for lithium-ion batteries modified by phenolic resin. J Power Sources. 2021; 483:229155. https://doi.org/10.1016/j.jpowsour.2020.229155

Accepted Manuscript

ACCEPTED MANUSCRIPT

[9] Gao K, Hu X, Yi T, Dai C. PE-g-MMA polymer electrolyte membrane for lithium polymer battery. Electrochim Acta. 2006; 52:443. https://doi.org/10.1016/j.electacta.2006.05.049

[10] Lee JY, Bhattacharya B, Nho YC, Park J. New separator prepared by electron beam irradiation for high voltage lithium secondary batteries. Nucl Instrum Methods Phys Res B. 2009; 267:2390-2394. https://doi.org/10.1016/j.nimb.2009.05.003

[11] Lee JY, Lee YM, Bhattacharya B, Nho YC, Park JK. Separator grafted with siloxane by electron beam irradiation for lithium secondary batteries. Electrochim Acta. 2009; 54:4312-4315. https://doi.org/10.1016/j.electacta.2009.02.088

[12] Kim KJ, Kim YH, Song JH, Jo YN, Kim JS, Kim YJ. Effect of gamma ray irradiation on thermal and electrochemical properties of polyethylene separator for Li ion batteries. J Power Sources. 2010; 195:6075-6080. https://doi.org/10.1016/j.jpowsour.2009.12.056

[13] Jiang Y, Sun C, Dong F, Xie H, Sun L. Multilayer polyethylene separator with enhanced thermal properties for safe lithium-ion batteries. Particuology. 2024; 91:29-37. https://doi.org/10.1016/j.partic.2023.12.017

[14] Lee Y, Ryou MH, Seo M, Choi JW, Lee YM. Effect of polydopamine surface coating on polyethylene separators as a function of their porosity for high-power Li-ion batteries. Electrochim Acta. 2013; 113:433-438. https://doi.org/10.1016/j.electacta.2013.09.104

[15] Kim JY, Lee Y, Lim DY. Plasma-modified polyethylene membrane as a separator for lithium-ion polymer battery. Electrochim Acta. 2009; 54:3714-3719. https://doi.org/10.1016/j.electacta.2009.01.055

ACCEPTED MANUSCRIPT

[16] Baek M, Yoo J, Kim Y, Jang YJ, Seo H, Lee SM, et al. Surface modification of polyethylene separator for Li-Ion batteries via imine formation. Int J Energy Res. 2023; https://doi.org/10.1155/2023/4624762

[17] Chen Z, Wang T, Yang X, Peng Y, Zhong H, Hu C. TiO_2 nanorod-coated polyethylene separator with well-balanced performance for lithium-ion batteries. Materials. 2023; 16:2049. https://doi.org/10.3390/ma16052049

[18] Dore MHI. Climate change and changes in global precipitation patterns: What do we know?. Environ Int. 2005; 31:1167-1181. https://doi.org/10.1016/j.envint.2005.03.004

[19] Pilapitiya PGCN, Ratnayake AS. The world of plastic waste: A review. Cleaner Mater. 2024;11:100220. https://doi.org/10.1016/j.clema.2024.100220

[20] Tarvydas D, Tsiropoulos I, Lebedeva N. Li-ion batteries for mobility and stationary storage applications – Scenarios for costs and market growth. European Commission: Joint Research Centre; 2018. https://doi.org/10.2760/87175

[21] Jian J, Xiangbin Z, Xianbo H. An overview on synthesis, properties and applications of poly(butylene-adipate-co-terephthalate)–PBAT. Adv. Ind Eng Polym Res. 2020; 3:19-26. https://doi.org/10.1016/j.aiepr.2020.01.001

[22] Ferreira FV, Cividanes LS, Gouveia RF, Lona MF. An overview on properties and applications of poly(butylene adipate-co-terephthalate)-PBAT based composites. Polym Eng Sci. 2019; 59:E7-E15. https://doi.org/10.1002/pen.24770

[23] Zhu B, Zhang W, Wang Q, Lai Y, Zheng J, Wen N, et al. Understanding the air-exposure degradation chemistry of the sacrificial cathode additive Li_5FeO_4 for Li-Ion batteries. Adv Funct Mater. 2024. https://doi.org/10.1002/adfm.202315010

[24] Søndergaard RR, Hösel M, Krebs FC. Roll-to-Roll fabrication of large area

Accepted Manuscript

ACCEPTED MANUSCRIPT

functional organic materials. J. Polym. Sci. B Polym. Phys. 2013; 51:16-34. https://doi.org/10.1002/polb.23192

[25] Montanino M, Sico G. Gravure Printing for Lithium-Ion Batteries Manufacturing: A Review. Batteries. 2023; 9:535. https://doi.org/10.3390/batteries9110535

[26] Lee H, Yanilmaz M, Toprakci O, Fu K, Zhang X. A review of recent developments in membrane separators for rechargeable lithium-ion batteries. Energy Environ Sci. 2014; 7:3857-3886. https://doi.org/10.1039/C4EE01432D

[27] Zhu M, Wang Q, Zhou H, Qi L. Binder-free TiO_2-coated polypropylene separators for advanced lithium-ion batteries. Energy Technol. 2020; 8:2000228. https://doi.org/10.1002/ente.202000228

[28] Prasanna K, Kim CS, Lee CW. Effect of SiO_2 coating on polyethylene separator with different stretching ratios for application in lithium ion batteries. Mater Chem Phys. 2014; 146:545-550. https://doi.org/10.1016/j.matchemphys.2014.04.014

[29] Babiker DMD, Usha ZR, Wan C, Hassaan MME, Chen X, Li L. Recent progress of composite polyethylene separators for lithium/sodium batteries. J Power Sources. 2023; 564:232853. https://doi.org/10.1016/j.jpowsour.2023.232853

[30] Nunes FC, Ribeiro KC, Martini FA, Barrioni BR, Santos JPF, Carvalho BM, et al. PBAT/PLA/cellulose nanocrystals biocomposites compatibilized with polyethylene grafted maleic anhydride (PE-g-MA). J Appl Polym Sci. 2021; 138:51342. https://doi.org/10.1002/app.51342

[31] Uehara GA, França MP, Junior SVC. Recycling assessment of multilayer flexible packaging films using design of experiments. Polímeros. 2015; 25:371-381. https://doi.org/10.1590/0104-1428.1965

ACCEPTED MANUSCRIPT

[32] Mousavi SM, Ahmadi S, Rasouli S, Fasihi M. Improving foamability and foam stability of poly(ethylene terephthalate) through chemical modification with styrene maleic anhydride. J Appl Polym Sci. 2024; 141:55930. https://doi.org/10.1002/app.55930

[33] Nam K, Kim SG, Kim DY, Lee DY. Enhanced mechanical properties of polylactic acid/poly(butylene adipate-co-terephthalate) modified with maleic anhydride. Polymers. 2024; 16:518. https://doi.org/10.3390/polym16040518

[34] Arruda LC, Magaton M, Bretas RES, Ueki MM. Influence of chain extender on mechanical, thermal and morphological properties of blown films of PLA/PBAT blends. Polym Test. 2015; 43:27-37. https://doi.org/10.1016/j.polymertesting.2015.02.005

[35] Tham DQ, Mai TT, Hoang T, Dung NTK, Tung NQ, Linh NTD, et al. Preparation and characterizations of plasticized PMMA/PVC/$Mg(ClO_4)_2$ electrolytes. VJST. 2019; 57:559-571. https://doi.org/10.15625/2525-2518/57/5/13661

[36] Rasouli S, Ataeefard M. Replacement of plasma-treated separators made of chain-extended poly(butylene adipate-co-terephthalate) with traditional environmentally harmful polymer-based membranes in lithium-ion batteries using gravure printing technique. J. Energy Storage. 2026; 148:120382. https://doi.org/10.1016/j.est.2026.120382

[37] Khalid Y, Achour A, Akram MA, Islam M. Polycarbonate/titania composites incorporating TiO_2 with different nanoscale morphologies for enhanced environmental stress cracking resistance in dioctyl phthalate. Polymers. 2022; 14:3693. https://doi.org/10.3390/polym14173693

[38] Wang J, Xu M, Yan J, Guo G, Wang Y, Zhang J, et al. Biodegradable poly(butylene adipate-co-terephthalate) (PBAT) modified by 1,4 cyclohexanedimethanol. Polymer.

Accepted Manuscript

ACCEPTED MANUSCRIPT

2024; 308:127348. https://doi.org/10.1016/j.polymer.2024.127348

[39] Davoodabadi A, Jin C, Wood DL III, Singler TJ, Li J. On electrolyte wetting through lithium-ion battery separators. Extreme Mech Lett. 2020; 40:100960. https://doi.org/10.1016/j.eml.2020.100960

[40] Pap AE, Dücső C, Kamarás K, Battistig G, Bársony I. Heavy water in gate stack processing. Mater Sci Forum. 2008; 573-574:119-31. https://doi.org/10.4028/www.scientific.net/msf.573-574.119

[41] Paxton NC, Woodruff MA. Measuring contact angles on hydrophilic porous scaffolds by implementing a novel raised platform approach: A technical note. Polym Adv Technol. 2022; 33:3759-3765. https://doi.org/10.1002/pat.5792

[42] Islam SMR, Park WY, Balasingam B. Unification of internal resistance estimation methods for Li-Ion batteries using hysteresis-free equivalent circuit models. Batteries. 2020; 6:32. https://doi.org/10.3390/batteries6020032

[43] Zhang Y, Du N, Yang D. Designing superior solid electrolyte interfaces on silicon anodes for high-performance lithium-ion batteries. Nanoscale. 2019; 11:19086-1910. https://doi.org/10.1039/C9NR05748J

[44] Zhao C, Niu J, Xiao C, Qin Z, Jin X, Wang W, et al. Separator with high ionic conductivity and good stability prepared from keratin fibers for supercapacitor applications. Chem Eng J. 2022;444:136537. https://doi.org/10.1016/j.cej.2022.136537

[45] Wang Z, Pan R, Xu C, Ruan C, Edström K, Strømme M, et al. Conducting polymer paper-derived separators for lithium metal batteries. Energy Storage Mater. 2018; 13:283-292. https://doi.org/10.1016/j.ensm.2018.02.006

[46] Wei N, Hu J, Zhang M, He J, Ni P. Cross-linked porous polymer separator using

ACCEPTED MANUSCRIPT

vinyl-modified aluminum oxide nanoparticles as cross-linker for lithium-ion batteries. Electrochim Acta. 2019; 307:495-502. https://doi.org/10.1016/j.electacta.2019.04.010

[47] Gong W, Gu J, Ruan S, Shen C. A high-strength electrospun PPESK fibrous membrane for lithium-ion battery separator. Polym Bull. 2019; 76:5451-5462. https://doi.org/10.1007/s00289-018-2631-4

[48] Na W, Koh KH, Lee AS, Cho S, Ok B, Hwang SW, et al. Binder-less chemical grafting of SiO_2 nanoparticles onto polyethylene separators for lithium-ion batteries. J Membr Sci. 2019; 573:621-627. https://doi.org/10.1016/j.memsci.2018.12.039

[49] Ma X, Zuo X, Wu J, Deng X, Xiao X, Liub J, et al. Polyethylene-supported ultra-thin polyvinylidene fluoride/hydroxyethyl cellulose blended polymer electrolyte for 5 V high voltage lithium ion batteries. J Mater Chem A. 2018; 6:1496-1503. https://doi.org/10.1039/C7TA08741A

[50] Gu L, Zhang M, He J, Ni P. A porous cross-linked gel polymer electrolyte separator for lithium-ion batteries prepared by using zinc oxide nanoparticle as a foaming agent and filler. Electrochim. Acta. 2018; 292:769-778. https://doi.org/10.1016/j.electacta.2018.09.147

[51] Zhang Y, Yuan JJ, Song YZ, Yin X, Sun CC, Zhu LP, et al. Tannic acid/polyethyleneimine-decorated polypropylene separators for Li-Ion batteries and the role of the interfaces between separator and electrolyte. Electrochim Acta. 2018; 275:25-31. https://doi.org/10.1016/j.electacta.2018.03.099

[52] Zhao H, Deng N, Yan J, Kang W, Ju J, Wang L, et al. Effect of OctaphenylPolyhedral oligomeric silsesquioxane on the electrospun Poly-m-phenylene isophthalamid separators for lithium-ion batteries with high safety and excellent

Accepted Manuscript

ACCEPTED MANUSCRIPT

electrochemical performance. Chem Eng J. 2019; 356:11-21. https://doi.org/10.1016/j.cej.2018.09.010

[53] Lin D, Yuen PY, Liu Y, Liu W, Liu N, Dauskardt RH, et al. A silica-aerogel-reinforced composite polymer electrolyte with high ionic conductivity and high modulus. Adv Mater. 2018; 30:1802661. https://doi.org/10.1002/adma.201802661

[54] Pereira RFP, Brito-Pereira R, Gonçalves R, Silva MP, Costa CM, Silva MM, et al. Silk fibroin separators: a step toward lithium-ion batteries with enhanced sustainability. ACS Appl Mater Interfaces. 2018; 10:5385-5394. https://doi.org/10.1021/acsami.7b13802

[55] Shanthi PM, Hanumantha PJ, Albuquerque T, Gattu B, Kumta PN. Novel composite polymer electrolytes of PVdF-HFP derived by electrospinning with enhanced Li-Ion conductivities for rechargeable lithium–sulfur batteries. ACS Appl Energy Mater. 2018; 1:483-494. https://doi.org/10.1021/acsaem.7b00094

[56] Liu J, Yang K, Mo Y, Wang S, Han D, Xiao M, et al. Highly safe lithium-ion batteries: High strength separator from polyformaldehyde/cellulose nanofibers blend. J Power Sources. 2018;4 00:502-510. https://doi.org/10.1016/j.jpowsour.2018.08.043

ACCEPTED MANUSCRIPT